Structural study of amorphous $Si_{1-y}Ni_y$:H alloys by EXAFS and infrared spectroscopy

1992 J. Phys.: Condens. Matter 4 7169

(http://iopscience.iop.org/0953-8984/4/35/003)

J. Phys.: Condens. Matter 4 (1992) 7169–7178. Printed in the UK

Structural study of amorphous $Si_{1-y}Ni_y$:H alloys by EXAFS and infrared spectroscopy

R Asal†, S H Baker†, S J Gurman†, S C Bayliss‡ and E A Davis†

† Department of Physics and Astronomy, University of Leicester, Leicester LE1 7RH, UK

‡ Department of Physics, Loughborough University of Technology, Loughborough, Leicestershire LE11 3TU, UK

Received 19 March 1992

Abstract. Atomic-scale structural changes with composition in sputtered amorphous a-$Si_{1-y}Ni_y$:H alloys with y varying from 0 to 1 have been studied by the x-ray absorption fine structure (EXAFS) technique. Complementary structural information from infrared (IR) spectroscopy has also been obtained. The EXAFS results indicate that there is a significant change in the local environment of the Ni atoms as their concentration is changed and the system appears to be chemically ordered, in the sense that the number of Ni–Ni bonds is minimized. The Si–Ni distance shows no significant variation with concentration and is the same as that found in crystalline nickel silicide. The Si–Ni Debye–Waller factors are also almost independent of composition. A correlation between these results and the infrared spectra is established.

1. Introduction

Interest in amorphous silicon alloys has quickened recently following the realization that, for example, the performance of solar cells made from these materials can be improved by tailoring the optical gap more closely to that of the solar spectrum [1]. Beside the transport and optical properties that have been studied, the semiconductor-to-metal transition is also of interest. The amorphous $Si_{1-y}Ni_y$:H system of present concern offers an example of a disordered system in which the band gap and electrical conductivity can be systematically controlled by changing the composition. Previous electrical and optical measurements have shown that the amorphous alloy exhibits a semiconductor-to-metal transition as a function of concentration at approximately $y = 0.26$ [2–4]. As y is increased up to this value, the absorption edge becomes very broad and only weakly dependent on photon energy. The optical gap, as determined by E_{O4} (the photon energy at which the absorption coefficient is 10^4 cm^{-1}), decreases with increasing nickel concentration and vanishes at $y = 0.26$. For $y > 0.26$, the reflectivity falls with increasing photon energy from 0.5 to 3 eV, characteristic of metallic-like Drude behaviour [3]. Analysis of far-UV reflectivity data has shown that the optical joint density of states (OJDOS) is, for $y > 0.26$, finite at all energies, implying that the conduction and valence bands overlap [4]. DC electrical measurements for $y \geqslant 0.26$ reveal a conductivity that varies as $\sigma = \sigma(0) - AT^m$, characteristic of metallic conduction, whereas for $y < 0.26$ the conductivity displays exponential behaviour ($\sigma = \sigma_0 \exp[-(T_0/T)^{1/2}]$), indicating variable-range hopping conduction

0953-8984/92/357169+10$04.50

in a Coulomb pseudogap at the Fermi level E_F [2]. Values of the optical conductivity show good agreement with the DC conductivity in the metallic regime [4].

The amorphous semiconductor–metal alloy $Si_{1-y}Ni_y$:H has also been shown to exhibit a semiconductor-to-metal transition as a function of pressure [5, 6]. The optical gap decreases with increasing pressure, becoming zero at pressures that are lower the higher the nickel content. The electrical conductivity at room temperature increases with applied pressure, reaching metallic values at a pressure that decreases with increasing nickel content.

In order to determine the local structural changes as the proportion of nickel is varied, the microstructure has been investigated as a function of composition using EXAFS and IR techniques. A preliminary report on the EXAFS measurements on a-$Si_{1-y}Ni_y$:H alloys ($y < 0.30$) has been published elsewhere [7]. The present investigation is an extension of the above study in that here the whole range of nickel concentration, from 0 to 100%, has been studied. Our conclusions differ somewhat from those reached in the earlier limited study. We also report on IR results for this system.

2. Experimental procedure

The a-$Si_{1-y}Ni_y$:H alloy films were prepared by radio-frequency co-sputtering in an argon–hydrogen atmosphere. The target consisted of a four-inch silicon wafer on which small pieces of 99.999% pure nickel were placed, the nickel concentration in the films being increased systematically by increasing the number of nickel pieces on the target. The actual percentage of nickel in the films was determined by energy-dispersive x-ray analysis (EDAX) using a DS 130 SEM. For EXAFS measurements the substrates were 2.0×10 cm^2 copper plates for the samples used for the silicon K-edge measurements and Mylar sheets for the nickel K-edge measurements. The substrates were mounted at a distance of 5.5 cm from the target and maintained at room temperature. The sputtering gas consisted of a mixture of argon and hydrogen at 5.5 mTorr pressure, the flow rates being 30 sccm for argon and 3.0 sccm for hydrogen. The RF power was 250 W which gave a deposition rate of about 1 μm in 6 h. The system base pressure was better than 4×10^{-7} Torr prior to introducing the gases. The films prepared under the conditions given above have an amorphous structure as indicated by electron diffraction and later confirmed by the EXAFS results, apart from the two most Ni-rich films with $y = 0.87$ and $y = 1.0$.

EXAFS measurements on both the nickel and silicon K edges were made at the SRS, Daresbury Laboratory (UK). The nickel-edge experiments were performed on beamline 7.1 in standard transmission geometry while the silicon-edge data were obtained on beamline 3.4 using the total electron yield method. A full technical description of each of these beamlines is available [8].

EXAFS mainly enables determination of the local structure around the absorbing atom, by extracting the following parameters: coordination number (N), nearest-neighbour distance (R) and Debye–Waller factor (σ^2). These parameters were obtained for our samples by multi-parameter fitting of experimental data to an EXAFS function calculated using the fast curved-wave theory [9]. The program used was the standard Daresbury package EXCURV88 [10]. A complete description of the data-fitting procedure can be found in our previous paper [7].

IR absorption measurements were performed using a double-beam Perkin–Elmer 580B spectrophotometer in the wavenumber range 180–2500 cm^{-1} (0.02–0.31 eV).

This system incorporates an air-filter unit to purge the sample compartment of water vapour and carbon dioxide which absorb in this region.

3. Results

3.1. EXAFS results

An example of EXAFS spectra obtained from x-ray absorption at the silicon K edge for a sample with $y = 0.2$ is shown in figure 1. Also shown is the radial distribution function (RDF) calculated by Fourier transformation of the EXAFS function. It is usual to treat the $\chi(k)$ data with a weighting scheme such as a k^3 one in order to compensate for amplitude reduction with increasing k. The Fourier transform is phase-corrected so that peaks appear at their true distances. In addition to the main peak lying between 2.0 and 2.5 Å, the Fourier transforms obtained from the Si K-edge data each show an additional peak between 1.0 and 2.0 Å. This is much more pronounced for the $y = 0.20$ sample. This is indicative of the presence of oxygen, since the Si–O bond length in SiO_2 is approximately 1.6 Å (we shall discuss this point later). However, in spite of this, which we believe arises from surface oxidation since it is observed in the surface-sensitive total electron yield data, we have still been able to analyse the Si-edge data. The amplitude factor $A(k)$, which corrects for events such as multiple excitations, and the so-called VPI parameter, which represents the photoelectron lifetime, were fixed at 0.85 and −4.0 eV respectively. Both values were obtained from analysis of a-Si:H and polycrystalline nickel samples. A parameter E_0 adjusts for the position of the absorption edge and was allowed to float freely.

The lengths of the Si–Si, Si–Ni and Ni–Ni bonds, as determined from the EXAFS, are plotted in figure 2. The Si–Si distances (determined only up to $y = 0.25$) are similar to that found in amorphous silicon (2.33 Å) but show a slight increase to approximately 2.39 Å with increasing y. This may be understood in terms of ionic repulsion between positively charged Si atoms, if one assumes charge transfer from silicon to nickel occurs. The Si–Ni distances, as measured from both Si and Ni edges, show no significant variation with composition, and within experimental error are the same as that found in crystalline nickel silicide $NiSi_2$ (2.33 Å). This suggests that the bond lengths are unaffected by the number and type of bonds surrounding each atom. The Ni–Ni distance is approximately 2.54 Å for $y \leqslant 0.21$ but then decreases rather abruptly to approximately 2.46 Å, which is similar to the value of 2.48 Å in metallic nickel [11]. It is possible that this change may reflect a change in the predominantly tetrahedral structure of the amorphous network to a higher-coordination metallic structure. Recently, the structure around Ni atoms in the interface layer of a Ni/a-Si:H system has been investigated using fluorescence EXAFS by Kawadzue *et al* [12]. They report bond lengths for Ni–Si and Ni–Ni of 2.35 Å and 2.46 Å respectively, in good agreement with our results.

The mean square deviation in nearest-neighbour distances (Debye–Waller factors), σ^2, are shown in figure 3. The Si–Si Debye–Waller factor for $y < 0.1$ is higher than that for amorphous silicon (45×10^{-4} Å^2) [13], but decreases with increasing y to approximately 25×10^{-4} Å^2 at $y = 0.2$. This reduction in the bond-length variation suggests that, at this value of y, there is less static disorder in the Si–Si distances than in pure a-Si. However, since the total electron yield measurements only probe the top 50–100 Å, this may be confined to the surface. The average measured value of σ^2 for the Si–Si bonds is equal to 60×10^{-4} Å^2. The room temperature thermal contribution

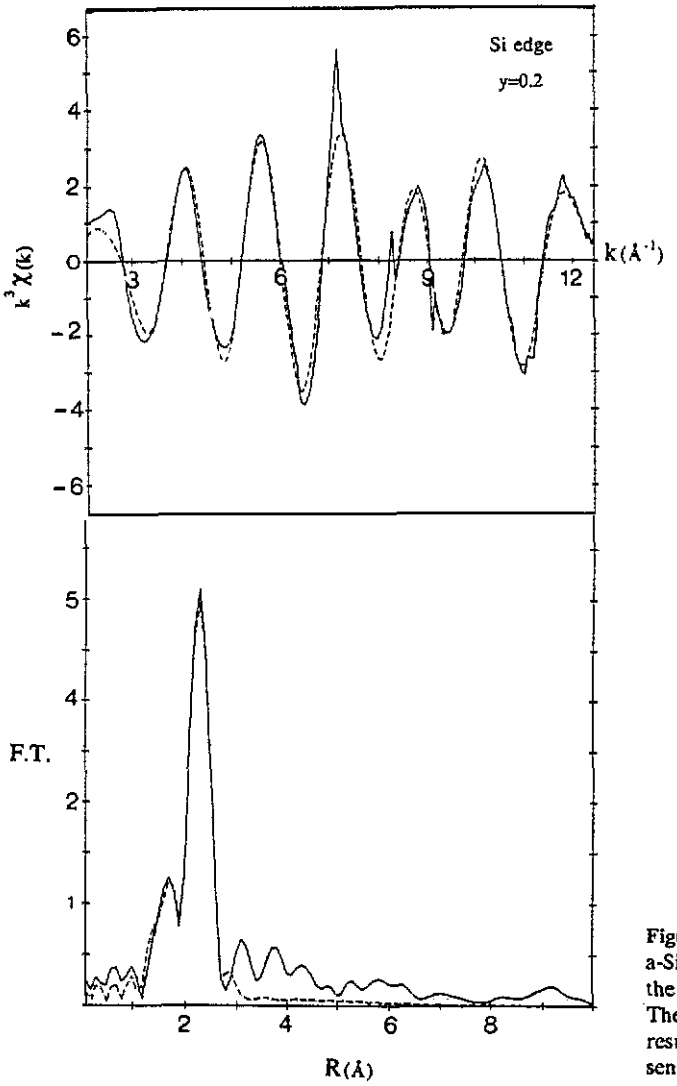

Figure 1. Typical EXAFS curve for the a-$Si_{1-y}Ni_y$:H sample ($y = 0.2$) with the corresponding Fourier transform. The solid curves are the experimental results and the broken curves represent the best fits to the data.

to σ^2 in the Si–Si bonds is equal to 40×10^{-4} Å^2 [13]. There is, therefore, little static disorder in the length of these bonds. We have found similar results for the Si–Si bond lengths in the a-$Si_{1-y}N_y$ and a-$Si_{1-y}O_y$ systems [14]. The Si–Ni and Ni–Ni Debye–Waller factors are almost independent of composition, suggesting that the disorder in these samples is similar over the whole composition range. The Debye–Waller factors for the Ni–Si bonds determined from both the Si and Ni edges are consistent with each other. The room temperature thermal contribution to σ^2 for the Si–Ni bond, as calculated using a method proposed by Cyvin in 1968 [15] with a stretch frequency of 680 cm^{-1}, is equal to 30×10^{-4} Å^2. Thus, there is a considerable static disorder in the Si–Ni bond length in our samples. Examination of the Debye–Waller factors for Ni–Ni indicates that there is no significant increase in the width of the distribution of Ni–Ni first-neighbour distances in the system. No second or higher shells could reliably be defined for samples with $y \leqslant 0.71$. However, this result is expected for

amorphous systems and suggests that there is a large amount of bond-angle variation in our samples and confirms the amorphous nature of films.

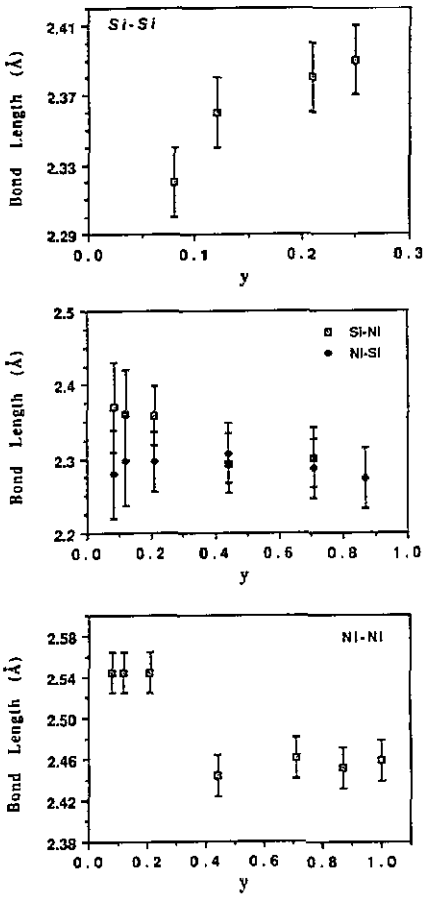

Figure 2. First-shell bond distances for different compositions of a-$Si_{1-y}Ni_y$:H alloys.

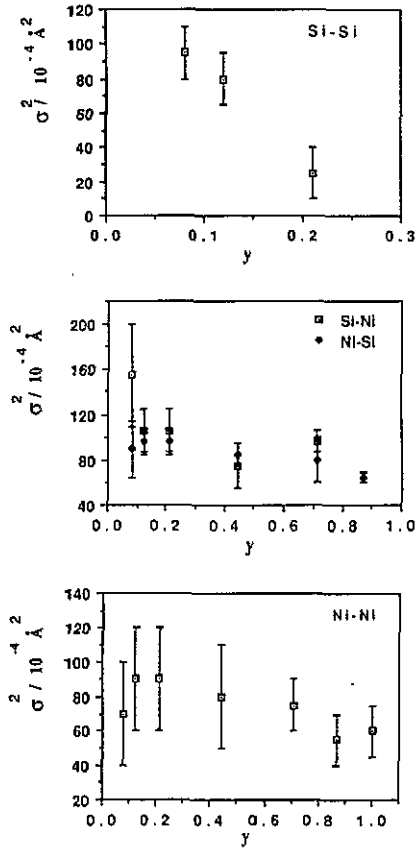

Figure 3. Composition dependence of the mean square deviation in interatomic distances, σ^2, obtained from the EXAFS data for a-$Si_{1-y}Ni_y$:H alloys.

Figures 4(*a*) and 4(*b*) show the silicon and nickel partial coordinations, and the total coordination number for both Si and Ni as a function of nickel concentration. Also shown in figure 4(*a*) are the partial coordinations of silicon expected for a random network and an ordered network, described later. It can be seen that the partial coordination number of silicon, N_{Si-Si}, decreases with increasing nickel and becomes undetectable for $y > 0.21$. This behaviour may be interpreted as the breakage of Si–Si bonds and the formation of Si–Ni bonds. This view is clearly supported by the associated increase in the Si–Ni coordination number. It should be noted that, within the error limits indicated, the total silicon coordination N_{total} is approximately 4.0 throughout the composition range studied. These results suggest the existence of a fourfold covalent environment for the silicon atoms. It must be emphasized that the total silicon coordination number is the sum of the silicon, nickel and oxygen atoms (we shall discuss the presence of the oxygen later).

However, EXAFS is too insensitive to reveal any possible total coordination changes due to hydrogen incorporation. A further weakness in the EXAFS technique for structure determination is that the coordination numbers and bond lengths determined here are averages over all possible structural units (i.e. bonding environments of Si) present in the samples. At the Si-rich end of the composition range, the Ni–Si coordination is high at approximately 8. This should be compared to the Ni coordination in c-$NiSi_2$, which adopts the CaF_2 structure, of 8. As the Ni content increases past stoichiometry ($y = 0.33$) into the Ni-rich region, the Ni–Ni coordination increases and finally reaches approximately 12 at 100% Ni, which is the value expected for a close-packed structure (Ni adopts a FCC structure). It should be mentioned that the 87% Ni and 100% Ni samples are polycrystalline. This was confirmed by the appearance of second and third shells in the RDFS for these two particular samples.

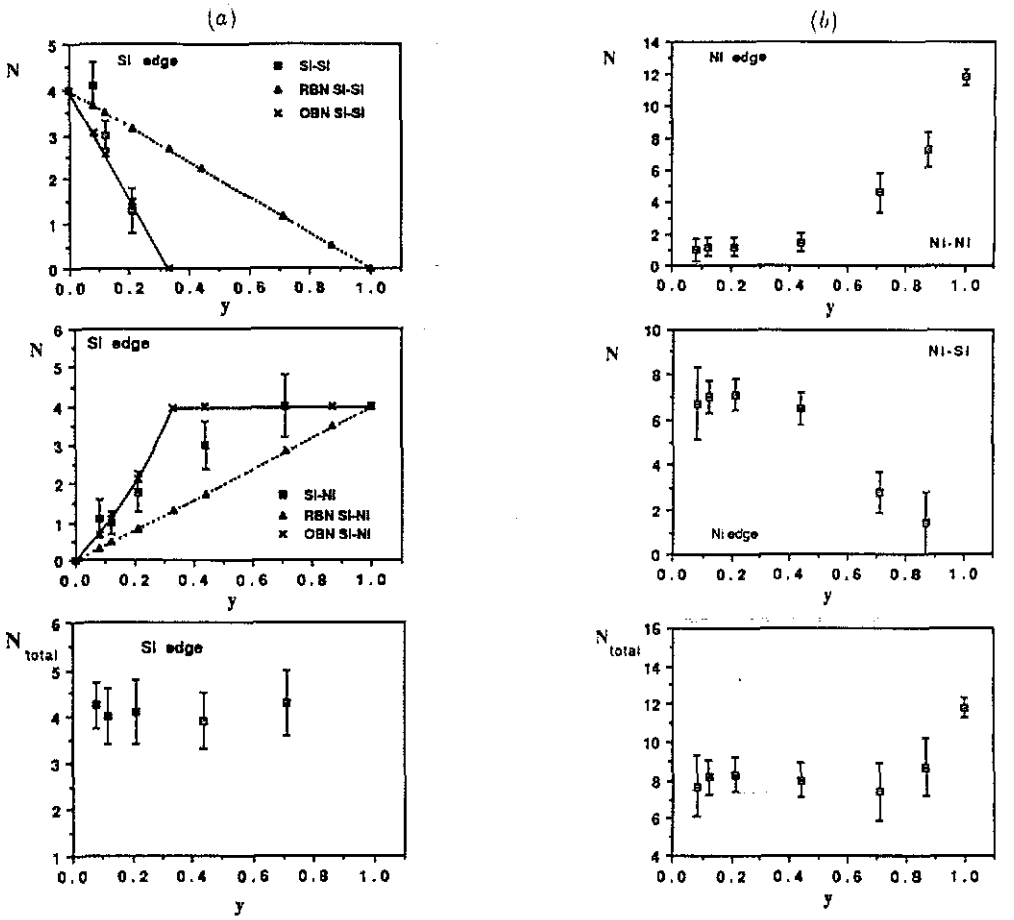

Figure 4. (*a*) Average first-shell Si coordination numbers obtained from silicon-edge data for a-$Si_{1-y}Ni_y$:H alloys as a function of composition. The solid line denotes the OBN model and the dotted line denotes the RBN model. (*b*) Average first-shell Ni coordination numbers obtained from nickel-edge data for a-$Si_{1-y}Ni_y$:H alloys as a function of composition.

The important point of interest here concerns the distribution of nickel in the amorphous silicon network, namely the degree of composition disorder. There are

two basic models that can be used to describe amorphous semiconductor alloys [16, 17]. The first is the random bond network (RBN) model. This neglects factors such as relative bond energies, so the distribution of bonds is purely statistical and is completely determined by the composition. The second model is the ordered bond network (OBN) model which assumes that bonds between unlike atoms are favoured, and complete chemical ordering occurs at the stoichiometric composition. For this model the number of bonds between unlike atoms is maximized at each composition. It can be seen in figure 4(*a*) that the partial coordination numbers of the Si atoms derived from the EXAFS measurement are similar to those calculated for the OBN model. This can be understood in terms of a chemically ordered arrangement in which the minority atom (Ni) is bonded only to Si atom and not to other Ni atoms. This is not perfectly so in view of the fact that a small, but not negligible, Ni–Ni coordination of approximately 1 is found at low y. The structure of a-$Si_{1-y}O_y$ was found to be chemically ordered, whereas the structure of a-$Si_{1-y}Ge_y$:H was in line with the RBN model [14, 29].

Amorphous silicon has the tetrahedral random network (TRN) structure [18] and shows semiconducting behaviour, while nickel adopts a dense random close-packed (DRP) structure, exhibiting typical metallic properties [19]. The fact that the total coordination of silicon at low nickel concentration ($y \leqslant 0.21$) is similar (within experimental error) to that of pure amorphous silicon suggests that the basic tetrahedral structure around Si atoms is still maintained in this concentration range. The Ni-edge EXAFS spectra (not shown) have a remarkably constant phase and a slowly decreasing amplitude with increasing nickel content, suggesting that the nickel environment is constant in this range. The system in this regime shows a semiconductor-like temperature dependence of electrical conductivity although the activation energy is reduced from that of pure amorphous silicon [2]. The optical gap (E_T or E_{04} at $y = 0.21$ remains finite (0.5 eV) and the reflectivity shows a behaviour typical of a semiconductor [3, 4]. All these indications are that the system is still a semiconductor with a tetrahedral structure for this range of concentration ($y \leqslant 0.21$). As the nickel concentration increases, the possibility for the silicon atoms to be bonded to more than one Ni atom increases (see figure 4(*a*)). Thus, it is reasonable to assume that the addition of Ni breaks the covalent bonds of amorphous Si, and that the tetrahedral covalent bonding around the Si atom changes to the eightfold metallic bonding around Ni atom. In such a metallic region with dense packing, four valence electrons per atom of silicon go into the conduction band and the 4s electrons of Ni would become non-localized states. The conduction band in Si–Ni alloys may be built up with a mixing of valence electrons of Si and Ni. As mentioned earlier (section 1), the system in this regime ($y > 0.26$) shows a metallic temperature dependence of electrical conductivity and the optical gap becomes zero. Measurements of x-ray diffraction in a similar system (GeNi) show that the structures of amorphous GeNi alloys for Ni concentrations over 30 at.% are similar to that in the liquid alloy and they become metallic [20]. This suggests that in such alloys the covalent bonds may even completely disappear. Neutron diffraction measurements on the GeNi system suggest that Ni (up to 30%) is incorporated substitutionally in a-Ge [21]. However, the data presented here cannot alone distinguish between the Ni being uniformly distributed, or the formation of domains of a-Si:H and Ni or $NiSi_2$ in clusters. Small-angle x-ray scattering (SAXS) studies for this system are in progress and should provide a clearer picture of the distribution of nickel atoms.

4. IR results

Infrared absorption spectra of sputtered a-$Si_{1-y}Ni_y$:H films are shown in figure 5. For films containing no nickel ($y = 0$), vibrational modes are seen at 2130, 1100, 890 and 630 cm^{-1}. These can be assigned as SiH_2 stretch (2130), SiH_2 bend (890), and SiH wag (630) modes [22]. A weak absorption band at 1100 cm^{-1} is assigned to the Si–O stretch mode. The IR absorption associated with the Si–Ni bonds is expected to be between 600 and 730 cm^{-1}, based on data for the diatomic molecule Si–Ni [23]. Thus, the Si–Ni IR band may overlap strongly with the SiH wag (630 cm^{-1}) mode band. This was confirmed with some films prepared without H_2 in the sputtering gas; a broad band at about 680 cm^{-1} was always observed and its intensity was comparable to, or larger than, that of the Si–H absorption. Other possibilities were eliminated by consulting the literature. The appearance of Si–Ni bonds is indicative of the presence of covalent bonds between Ni and Si at these concentrations ($y = 0.44$ and $y = 0.71$).

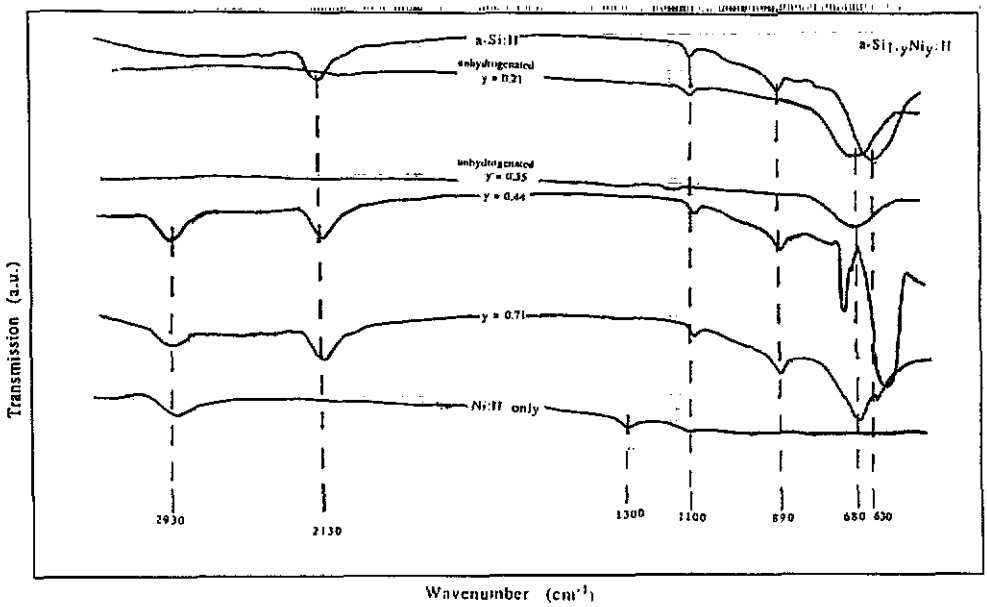

Figure 5. Infrared absorption spectra of a-$Si_{1-y}Ni_y$:H for various values of y.

As can be seen from figure 5, the position of the Si:H wagging mode is altered on addition of the metal, indicating that the Ni and H are bonded to the same Si atom. Previous work on Ni^+-ion-implanted a-Si [24] suggests that direct saturation of dangling bonds with the metal takes place. The gradual replacement of H atoms in Si–H bonds by Ni atoms should lead to the eventual disappearance of Si–H bonds, as observed in the present films. This may provide evidence that the films are homogeneous. EDAX measurements performed at the Cavendish Laboratory did not show any inhomogeneity beyond experimental error.

We find evidence for Ni–H bonds, which probably occur at wavenumbers between 2500–3000 cm^{-1} [23]. The appearance of Ni–H bonding at $y = 2930$ cm^{-1} is indicative of the presence of a number of Ni dangling bonds, which are readily passivated by hydrogen, and it also shows that H bonds to both silicon and nickel, although

preferably to silicon. A preference ratio of about 10 for Si–H bonds compared to Ge–H bonds was observed in a-SiGe:H alloys [25]. The ratio is likely to be higher for a-$Si_{1-y}Ni_y$:H. A similar observation has been reported in the case of RF-sputtered a-$Si_{1-x}Sn_x$:H films for $x < 0.5$ [26]. The weak absorption band at 1300 cm^{-1}, for the film with $y = 1$, is assigned to a Ni–O stretch mode.

A remark is made here concerning the presence of oxygen in our samples. It is likely that most of the oxygen contamination is a result of post-deposition oxidation because of the following observations: (i) the fact that oxygen is detected by the surface measurements technique of the station 3.4 but not by transmission measurements at station 7.1 indicates that the oxygen is present as an oxide surface layer, rather than distributed through the film; (ii) the wavenumber corresponding to the IR oxide signal from the surface is between 1040 and 1080 cm^{-1} [27], whereas the wavenumber corresponding to the oxygen incorporated during growth is between 930 and 1020 cm^{-1} [28]. The Si–O vibration mode in our samples appears at a wavenumber of approximately 1100 cm^{-1}. This implies the absorption of oxygen on the sample surface after deposition.

5. Summary

The atomic scale structure of a-$Si_{1-y}Ni_y$:H has been investigated over a wide composition range by EXAFS and IR techniques. It is concluded that a chemically ordered network model provides the best fit to the data. Values obtained for the Si–Si bond length lie in the range 2.32–2.39 Å, which is similar to the value of 2.33 Å for a-Si:H. The Si–Ni bond length shows no significant variation with composition and is the same as that found in crystalline nickel silicide. The Debye–Waller factors for Si–Ni determined from both the Si and Ni edges are consistent with each other and do not vary appreciably with composition. There is a considerable static disorder in the Si–Ni bond length but little in the length of the Si–Si bond. IR results show that the nickel bonds to both silicon and hydrogen, from the appearance of a Si–Ni vibrational mode at 680 cm^{-1} and a Ni–H mode at 2930 cm^{-1}.

Acknowledgments

The authors are grateful to the SERC for provision of synchrotron radiation and computing facilities at the Daresbury Laboratory. The bulk of the work was made possible by grants from the SERC. R Asal wishes to thank the Ministry of Higher Education (MoHE) in Iraq for the award of a studentship.

References

[1] Hamakawa Y 1982 *Amorphous Semiconductors: Technologies and Devices* (Amsterdam: North-Holland)

[2] Abkemeier K, Adkins C J, Asal R and Davis E A 1992 *Proc. 4th Int. Conf. on Hopping and Related phenomena (Marburg, 1991);* 1992 *Phil. Mag.* **65** 675

[3] Davis E A, Bayliss S C, Asal R and Manssor M 1989 *J. Non-Cryst. Solids* **114** 465

[4] Bayliss S C, Asal R, Davis E A and West T 1991 *J. Phys.: Condens. Matter* **3** 793

[5] Asal R, Bayliss S C and Davis E A 1991 *Proc. 20th Int. Conf. on the Physics of Semiconductors (Thessaloniki, Greece, 6–10 August 1990)* vol 3, ed E M Anastassakis and J D Joannopoulos (Singapore: World Scientific) p 2091
[6] Asal R, Bayliss S C and Davis E A 1991 *J. Non-Cryst. Solids* **137 & 138** 931
[7] Edwards A M, Fairbanks M C, Newport R J, Gurman S J and Davis E A 1989 *J. Non-Cryst. Solids* **113** 41
[8] Morrell C, Campbell J C, Diakun G P, Dobson B R, Greaves G N and Hasnain S S *EXAFS User Manual* SERC Daresbury, UK
[9] Gurman S J, Binsted N and Ross I 1984 *J. Phys. C: Solid State Phys.* **17** 143
[10] Binsted N, Gurman S J and Campbell J W 1988 *EXCURV88 program* SERC Daresbury, UK
[11] Ovshinsky S R 1977 *Amorphous and Liquid Semiconductors* ed W E Spear (Edinburgh: University of Edinburgh Press
[12] Kawadzu Y, Iioka M and Fujii M 1989 *Appl. Surf. Sci.* **41/42** 296
[13] Bayliss S C and Gurman S J 1991 *J. Non-Cryst. Solids* **127** 174
[14] Singh A, Bayliss S C, Gurman S J and Davis E A 1992 *J. Non-Cryst. Solids* **142** 113
[15] Cyvin S J 1968 *Molecular Vibrations and Mean Square Amplitudes* (Amsterdam: Elsevier)
[16] Philipp H R 1972 *J. Non-Cryst. Solids* **8** 627
[17] Gurman S J 1990 *J. Non-Cryst. Solids* **125** 151
[18] Polk D E 1971 *J. Non-Cryst. Solids* **5** 365
[19] Polk D E 1972 *Acta. Metall.* **20** 485
[20] Tamura K and Fukushima J 1973 *The Properties of Liquid Metal* ed S Takeuchi (London: Taylor and Francis)
[21] Yamada K, Endoh U, Ishikawa U and Watanabe N 1980 *J. Phys. Soc. Japan* **48** 922
[22] Brodsky M H, Cardona M and Cuomo J J 1977 *Phys. Rev.* B **16** 3556
[23] See for example,
Nakamoto K 1978 *Infrared and Raman Spectra of Inorganic and Coordination Compounds* (New York: Wiley)
[24] Dvurechenskii A V, Dravin V A and Ryazantsev I A 1986 *Phys. Status Solidi* **95** 635
[25] Paul W, Paul D K, van Roedern B, Blake J and Oguz S 1981 *Phys. Rev. Lett.* **46** 1016
[26] Vergnat M, Piecush M, Marchal G and Gerl M 1985 *Phil. Mag.* B **51** 327
[27] Anderson D A, Moddel G, Poester M A and Paul W 1979 *J. Vac. Sci. Technol.* **16** 906
[28] Yacobi B G, Collins R W, Moddel G, Viktorovitch P and Paul W 1981 *Phys. Rev.* B **24** 5907
[29] Asal R, Bayliss S C, Gurman S J and Davis E A *in preparation*